Bull. Mater. Sci., Vol. 31, No. 7, December 2008, pp. 967–973. © Indian Academy of Sciences.

Preparation, characterization and luminescent properties of europium oxide doped nano $LaMn_{0.9}Zn_{0.1}O_{3+d}$ by sol–gel processing

ABDOLALI ALEMI*, ELNAZ KARIMPOUR and HOSSEIN SHOKRI
Department of Inorganic Chemistry, University of Tabriz, Tabriz 51667, Iran

MS received 17 May 2008; revised 18 July 2008

Abstract. **New compounds of rare earth complex oxides with perovskite structure in a combination of La with Eu ions and Mn with Zn ions, $La_{1-x}Eu_xMn_{0.9}Zn_{0.1}O_{3+d}$ (LEMZ) ($0.0 \le x \le 0.32$) in A and B sites, respectively were synthesized. X-ray powder diffraction (XRD), fourier transform infrared spectroscopy (FT–IR) and photoluminescence spectra (PL) were used to characterize the resulting nanoparticles. The powder X-ray diffraction peaks could be indexed as a rhombohedral cell. The results of FT–IR spectra were in agreement with those of XRD. High-quality nanopowders with controlled stoichiometry and microstructure were prepared at a temperature range of 700–800°C for 6 h, with mean particle sizes of ~ 17·5 nm. Photoluminescence measurements showed Eu^{3+} ions characteristic red emission in crystalline LEMZ powders due to the $^5D_0 \rightarrow {}^7F_J$ ($J = 0$–6) transitions of the 4*f* electrons of Eu^{3+} ions. The structure, homogeneity and particle size of the obtained compounds during different stages were investigated by scanning electron microscopy (SEM).**

Keywords. **Lanthanum; manganese; europium; perovskite; sol–gel; luminescence.**

1. Introduction

In recent years, a lot of work has been done on nanocrystalline materials because of their unusual properties of bulk materials (Rondinone *et al* 2000). On the other hand, perovskite-type oxides (general, formula ABO_3) have been attracting much attention for more than two decades due to their potential commercial applications as catalysts for various reactions (Eraoka *et al* 2000), and high technological importance because of their interesting electronic (El-Fadli *et al* 2002) and magnetic (Zheng *et al* 2006) properties. More recently, the perovskite manganite compounds have received much attention because of their colossal magnetoresistance (CMR) (Ramesha *et al* 1998) that result from the presence of Mn^{4+} ions and charge ordering properties (Raveau *et al* 2001).

The properties of perovskite-type oxides, of general formula, ABO_3, depend tightly on the nature of A and B ions and on the valence state of A and B. The A site ions are in general catalytically inactive and influence thermal stability of perovskite, while the transition metal ions at B position are active components. By replacing part of A or B ions with A′ and B′, respectively, it is possible to create or suppress oxygen vacancies on the catalysts. The effect of the A site vacancies is quiet different from that produced by the B site ones. It is well known that the A-site doping can change structural, electronic and magnetic properties of perovskite manganites. And properties depend crucially on the doping level as well as the nature of the doping element (Marchetti and Forni 1998).

Lanthanum manganese mixed oxide of formula, $LaMnO_{3\pm d}$, as a perovskite, can be an appropriate host lattice for other rare earth ions, alkaline metal ions and alkaline earth metal ions and it means that metal ions can be located in its lattice and produce new properties. The limits of tolerance factor, $t = (A–O)/\sqrt{2}(M–O)$, where A–O and M–O are the bond lengths for many metallic elements are responsible for providing perovskite structure in this kind of ceramics (Whangbo *et al* 2002).

Research has recently given evidence that the substitution of Mn or La for another ion directly modifies the chemical and physical properties, because of altering interactions in the La–O and Mn–O networks.

Various methods have been tested to synthesize lanthanum manganite, $LaMnO_{3+d}$, including the conventional solid-state reaction (Inaguma *et al* 2006), co-precipitation (Philip and Kutty 2000), sol–gel (Gaudon *et al* 2002; Alemi *et al* 2008), hydrothermal synthesis (Zenati *et al* 2005) and molten salts reactions.

$LaMnO_3$ perovskite crystallizes in the *Pbnm* structure where the manganese atom is surrounded by distorted oxygen octahedral. This compound develops an antiferromagnetic ordering at 140 K, showing weak ferromagnetism due to spine canting. Synthesis in oxidation conditions gives rise to the formation of the $LaMnO_{3+d}$ series. The oxygen excess *d*, which cannot be accommodated in the lattice, results in equal amounts of La and Mn vacancies.

*Author for correspondence (alemi@tabrizu.ac.ir)

The series shows a continuous evolution from the highly distorted orthorhombic structure of $LaMnO_3$ towards a rhombohedral structure for $d = 0{\cdot}15$ sample. This structural change is coupled with an enhancement of the ferromagnetic interaction. Therefore, $LaMnO_{3{\cdot}07}$ is a ferromagnetic compound, but having neither a metal–insulator transition nor a giant magnetically inhomogeneous compound showing a spin-glass state at low temperatures. A number of detailed investigations have shown that the synthesis temperature and the oxygen partial pressure control the Mn^{3+}/Mn^{4+} ratio in $LaMnO_{3+d}$ oxides (Subias *et al* 1999).

In this paper, we present a simple Pechini-type polymerizable complex (PC) route, based on polyesterification between citric acid (CA) and ethylene glycol (EG), that has been successfully used to synthesize several compounds with perovskite structure including lanthanum manganite-based oxides at relatively low temperatures. Some other methods have been utilized for the preparation of $LaMnO_{3+d}$ at reduced temperatures with various degrees of success (Giannakas *et al* 2004; Reddy *et al* 2006). But the advantages of sol–gel method is, therefore, to use another solution route, that enables the low temperature synthesis of smaller grained powders of phase-pure, $LaMnO_{3+d}$, with relatively high surface area. A set of complementally investigative methods have been used to characterize the obtained ceramics. Structural analysis has been evaluated by X-ray diffraction (XRD) and its particle sizes were investigated by scanning electron microscopy (SEM).

2. Experimental

Europium doped $LaMn_{0{\cdot}9}Zn_{0{\cdot}1}O_{3+d}$ were prepared by Pechini sol–gel method (Alemi *et al* 2008) employing the corresponding metal nitrates and Eu_2O_3 weighed and dissolved in acid to form europium nitrate. Then aqueous solutions of metal nitrates with nominal atomic ratios La : Eu : Mn : Zn = $(1 - x)$: x : 0·9 : 0·1, with x = 0·00, 0·1, 0·2, and 0·32 were mixed together in de-ionized water to give a concentrated solution. The exact quantities of La, Eu, Mn and Zn in the metal nitrates were determined by thermogravimetric analysis. Citric acid was then proportionally added to the metal solution to have the same amounts of equivalents. The solution was concentrated by evaporation at ~60°C with stirring for 2 h to convert them to stable (La, Mn)/CA complexes. Then ethylene glycol was added to this solution as a cross-linking agent. The solution thus prepared, while being stirred with a magnetic stirrer, was heated at ~90°C to remove excess water and subsequently to accelerate polyesterification reactions between CA and EG. The heating at ~90°C produced a viscous, bubbly mass that formed a brown resin upon cooling. During the evaporation of the solvent, a reddish-brown gas corresponding to NO_2 comes out of the solution. This NO_2 departure occurs mostly at the end of evaporation and is very exothermic. Charing the resin at 450°C for 2 h resulted in a solid mass, which was lightly ground into powder with an agate mortar. In this step of calcinations, brown smoke and NO_x gas evolution, was again observed. To fully evaporate highly combustion species in the mass and to burn down most of the organic constituents the powder was calcined in a furnace at 800°C in static air for 6 h. The annealing of the amorphous precursor at 800°C allows to remove most of the residual carbon, and to obtain the rhombohedral perovskite phase with the $R3C$ space group. A typical flow chart for the preparation of LEMZ by sol–gel processing is shown in figure 1.

The chemical reaction taking place during the process is given below:

$$La(NO_3)_{3(aq.)} + Eu(NO_3)_{3\,(aq.)} + Zn(NO_3)_{2\,(aq.)} + Mn(NO_3)_{2\,(aq.)} + (C_6H_5O_7)_{(aq.)} + (CH_3O)_2 \xrightarrow{90^\circ C}$$

$$\text{metal nitrate-CA/EG polyester network} \xrightarrow{800^\circ C}$$

$$La_{1-x}Eu_xMn_{0{\cdot}9}Zn_{0{\cdot}1}O_{3+d(s)} + xNO_{2(g)} + xCO_{2(g)} + xH_2O_{(g)}$$

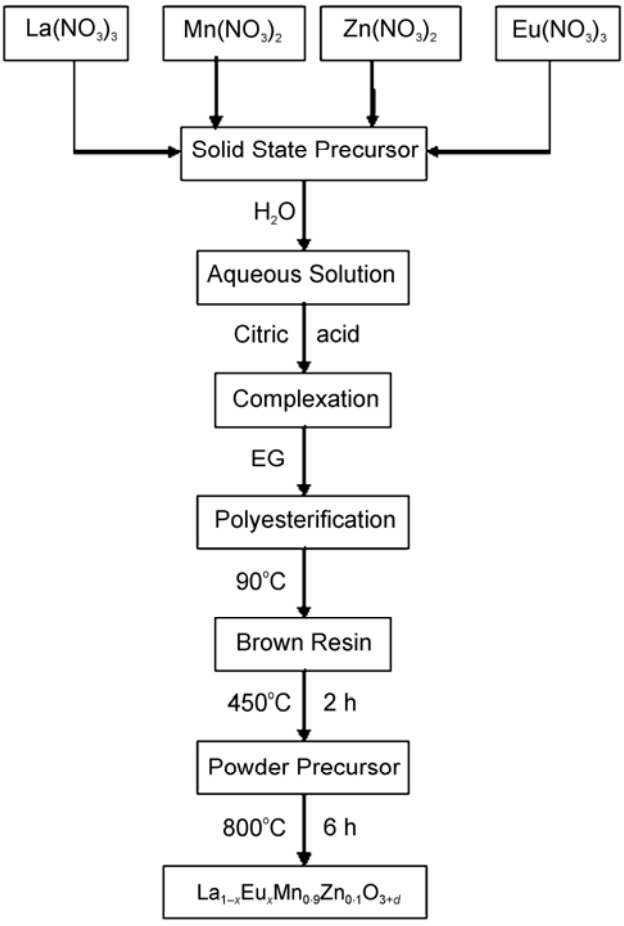

Figure 1. Flow chart for preparing $La_{1-x}Eu_xMn_{0{\cdot}9}Zn_{0{\cdot}1}O_{3+d}$ by the Pechini method.

The X-ray powder diffraction (XRD) measurements were carried out with D5000 Siemens with Cu-K_α line of wavelength, $\lambda = 1{\cdot}541$ Å at the scanning rate of 2°/min and 2θ was varied from 15° to 65°. The FT–IR transmission spectra in the region 400–4000 cm^{-1} were recorded for all the samples using FT–IR Nexus 670 by KBr pellet technique. The scanning electron microscope (SEM) images were performed by means of a Jeol JEM-100 CXII microscope. The photoluminescence (PL) excitation and emission spectra were taken on a Cray Eclipse spectrofluorimeter.

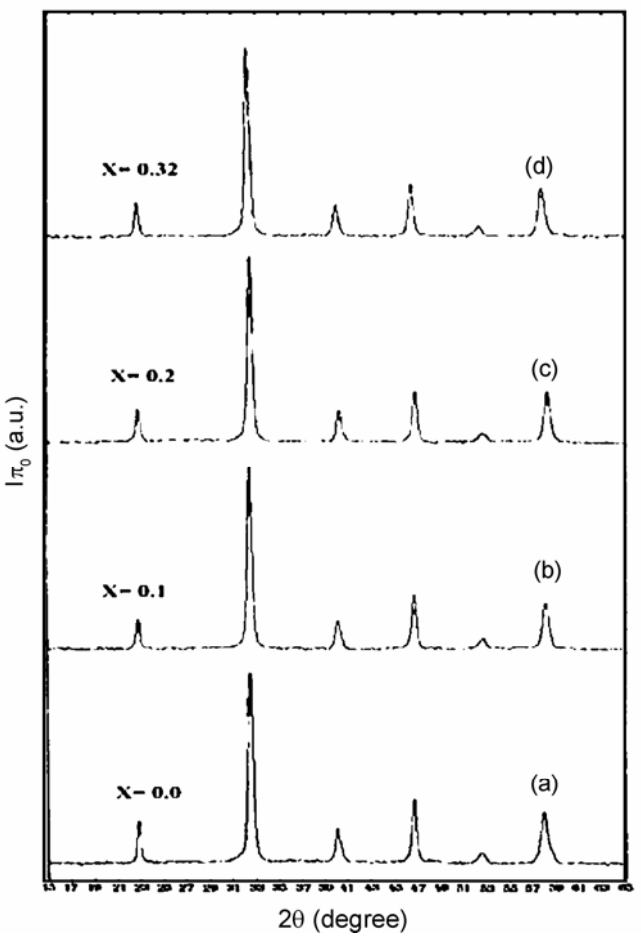

Figure 2. X-ray diffractogram of $La_{1-x}Eu_xMn_{0.9}Zn_{0.1}O_{3+d}$ calcined at 800°C: (a) $x = 0{\cdot}0$; (b) $x = 0{\cdot}1$; (c) $x = 0{\cdot}2$ and (d) $x = 0{\cdot}32$.

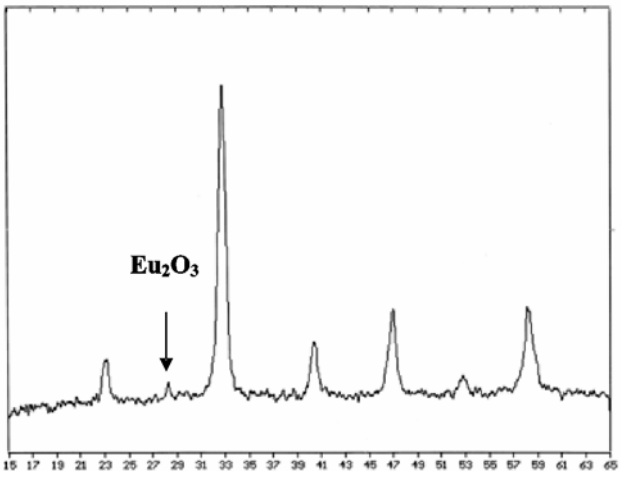

Figure 3. X-ray diffraction pattern of $La_{1-x}Eu_xMn_{0.9}Zn_{0.1}O_{3+d}$ for $x = 0{\cdot}4$.

3. Results and discussion

3.1 *X-ray diffraction studies*

XRD analyses have been made on $LaMn_{0.9}Zn_{0.1}O_{3+d}$ and $La_{1-x}Eu_xMn_{0.9}Zn_{0.1}O_{3+d}$ with various europium contents calcined at 800°C in air for 6 h, respectively. X-ray diffraction patterns of figure 2 show that the limit of europium incorporation is $x = 0{\cdot}32$. Indeed, for $x = 0{\cdot}4$, the presence of Eu_2O_3 phase is detected on diffraction patterns (figure 3). They show that all samples are single phase with no detectable secondary phases and these samples can be indexed with the rhombohedral structure with the space group $\bar{R}3C$ (Porta *et al* 1999). According

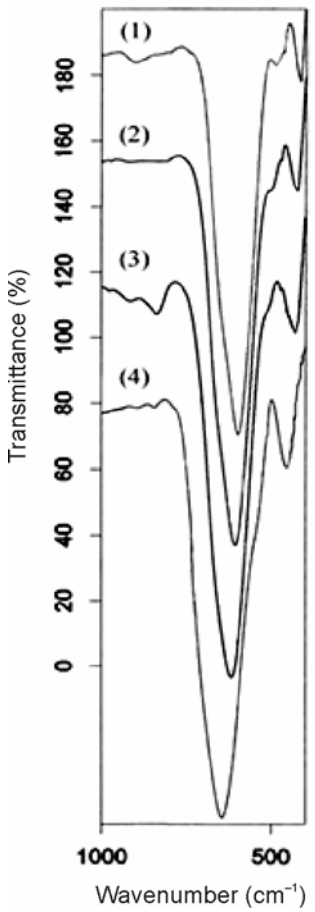

Figure 4. FTIR spectra of $La_{1-x}Eu_xMn_{0.9}Zn_{0.1}O_{3+d}$: (1) $x = 0{\cdot}0$; (2) $x = 0{\cdot}1$; (3) $x = 0{\cdot}2$ and (4) $x = 0{\cdot}32$.

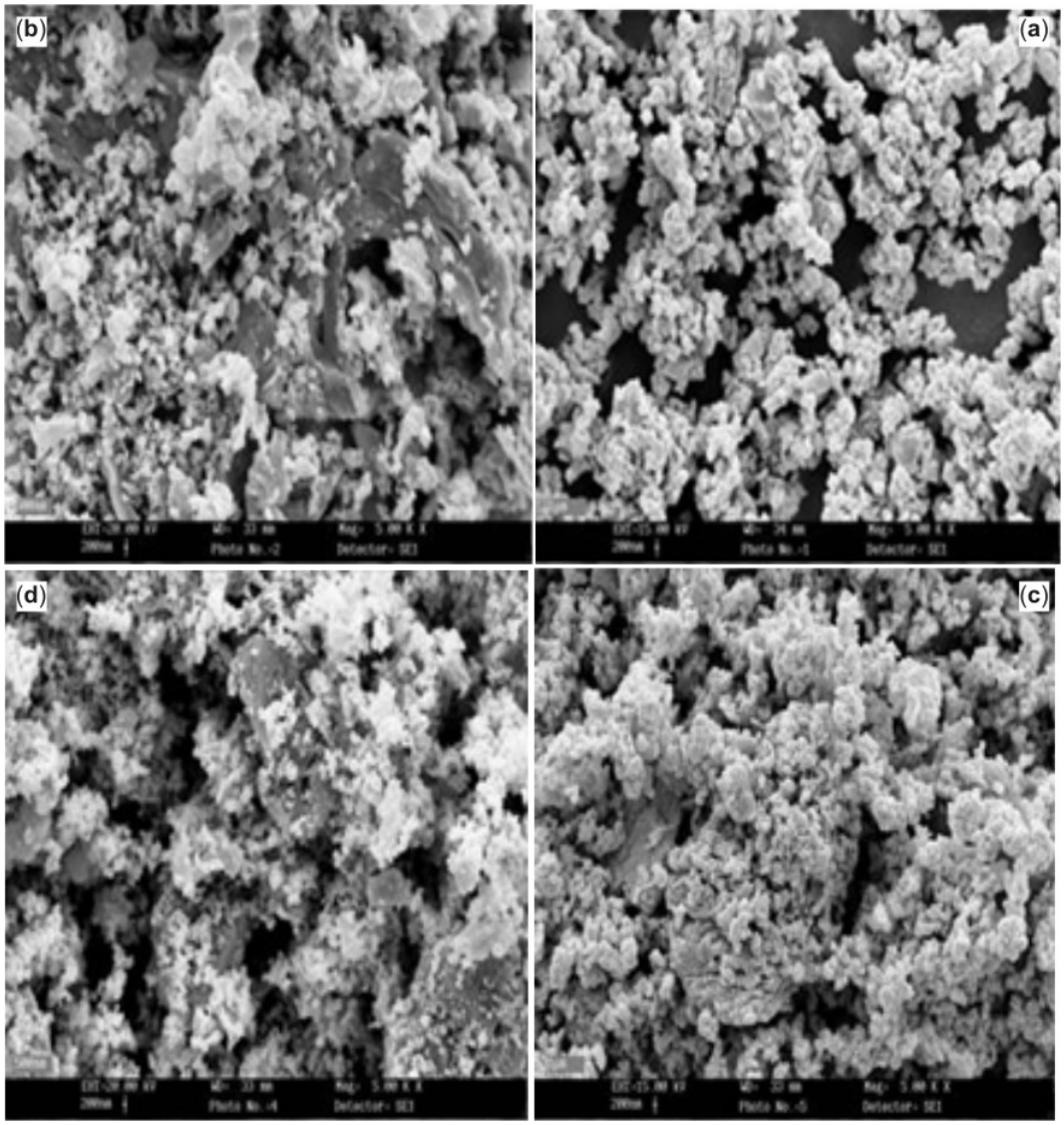

Figure 5. SEM images of (**a**) $LaMn_{0.9}Zn_{0.1}O_{3+d}$, (**b**) $La_{0.9}Eu_{0.1}Mn_{0.9}Zn_{0.1}O_{3+d}$, (**c**) $La_{0.8}Eu_{0.2}Mn_{0.9}Zn_{0.1}O_{3+d}$ and (**d**) $La_{0.68}Eu_{0.32}Mn_{0.9}Zn_{0.1}O_{3+d}$ calcined at 800°C in air.

Table 1. Average particle size ($La_{1-x}Eu_xMn_{0.9}Zn_{0.1}O_{3+d}$) was determined by scanning electron microscopy, that are in good agreement with the XRD results: (pure phase) $x = 0{\cdot}0$; (a) $x = 0{\cdot}1$; (b) $x = 0{\cdot}2$ and (c) $x = 0{\cdot}32$.

Sample	t(nm)
Pure-phase	19/5787
a	19/4625
b	17/1495
c	14/0707

to literature data, the maximum incorporation rate seems to be influenced by the ionic radius of the substituted cation.

As shown in figure 2, the X-ray diffraction patterns of all samples indicate that a single phase of the perovskite-type structure was formed. No extra peaks were observed, indicating the absence of secondary phases. Also noticeable is the absence of peak shifts from $LaMn_{0.9}Zn_{0.1}O_{3+d}$ to europium doped samples, indicating no significant variation on the volume of the unit cell.

The crystallite size, D_{hkl}, of the samples prepared at 800°C to the peak at $2\theta = 33°$ was calculated from the main reflection of the rhombohedrally-distorted perovskite by means of the Debye–Scherrer equation (Vazquez-Vazquez and Lopez-Quintela 2006):

$$D_{110}\,(\text{Å}) = k\lambda/\beta\cos\theta,$$

where k is a shape factor which normally ranges between 0·9 and 1·0 (in our case, $k = 0{\cdot}9$), λ the X-ray wavelength (Cu-K_{α_1}, $\lambda = 1{\cdot}54060$ Å), and θ the Bragg angle. B is the difference in profile widths of broadened and standard

samples (in our case, a silicon standard was used): $\beta = \beta_{sample} - \beta_{standard}$, β being the integral breadth defined as β = area (Cu-K_{α_1})/intensity (Cu-K_{α_1}).

Phase analysis revealed for the samples, the presence of a single perovskite phase with primitive rhombohedral symmetry and $\bar{R}3C$ space group up to $x = 0{\cdot}32$ (figure 2). All the diffraction lines could be indexed and no impurity lines due to lanthanum oxide, europium oxide, zinc oxide or any of the known oxides of Mn, such as Mn_2O_3, Mn_3O_4 and MnO_2, were seen. No extra peaks were observed indicating the absence of secondary phases.

The average crystalline size of ~ 17·5 nm for Eu doped systems were determined from the X-ray diffraction peak at $2\theta \approx 31$–33°, by means of the Scherrer equation.

3.2 *Infrared spectral studies*

Chemical and structural changes and the formation of desired crystal phases during the combustion process can be observed by infrared spectroscopic analysis. FT–IR spectra of the europium doped $LaMn_{0.9}Zn_{0.1}O_{3+d}$ is shown in figure 4.

However, the main absorption is located at 602·67 cm^{-1} and it is assignable to the metal–oxygen stretching in the perovskite that corresponds to Mn–O stretching vibration here (Porta *et al* 1999).

All the absorption bands were assigned to those of the perovskite structure, and it seems that in the spectra containing different concentrations of europium oxide the structure is not changed. With the increase of Eu doping content from $x = 0$ to $x = 0{\cdot}32$, the frequency of IR absorption peaks at 602·67, 497·38 and 423·10 cm^{-1} shift slightly up to a higher frequency for LEMZ systems. The shift detected corresponds to presence of Eu–O bond in compounds.

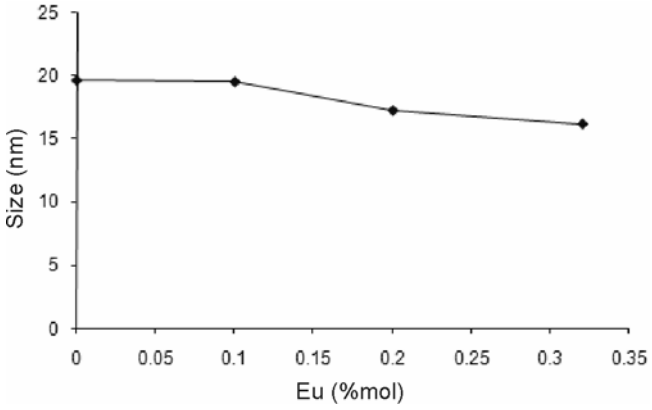

Figure 6. Particle sizes of $La_{1-x}Eu_xMn_{0.9}Zn_{0.1}O_{3+d}$ calcined at 800°C versus molar ratio of Eu^{3+}. Average particle diameter decreases with increasing europium content.

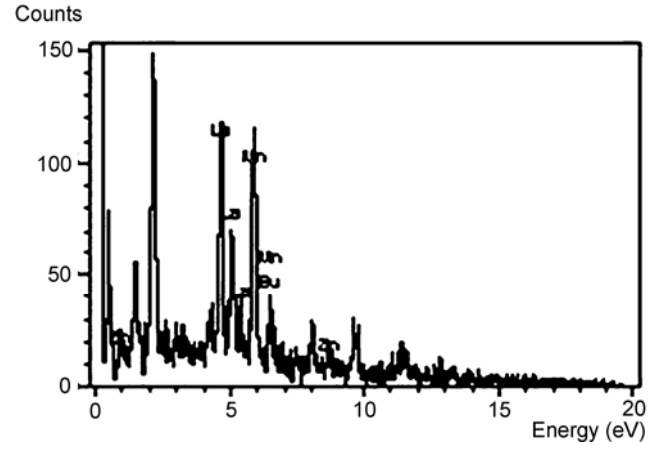

Figure 7. Energy dispersive spectra (EDX) of $La_{0.68}Eu_{0.32}Mn_{0.9}Zn_{0.1}O_{3+d}$.

3.3 *Microstructural analysis*

The SEM micrographs of $LaMn_{0.9}Zn_{0.1}O_{3+d}$ and its doped systems with various europium contents are shown in figure 5, respectively. In $LaMn_{0.9}Zn_{0.1}O_{3+d}$ (figure 5a), these are composed of spherical and agglomerated particles of ~ 20 nm diameter.

The SEM micrographs indicate the distribution of uniform grains with spherical shape. Figures 5b–d indicate SEM photograph of $La_{1-x}Eu_xMn_{0.9}Zn_{0.1}O_{3+d}$ with $x = 0{\cdot}1$, 0·2, 0·32, respectively and shows that the particle sizes of the samples prepared at 800°C for 6 h in air are distributed uniformly. In all the samples, micrograph shows homogeneous nanostructure and uniform particles, having sizes between about 15 and 20 nm. The average particle size was determined by scanning electron microscopy (table 1). Micrographs show that particles with an average size as small as 17·5 nm were synthesized for LEMZ nano powders calcined at 800°C. This is confirmed by X-ray diffraction spectra of LEMZ nano powders which displayed broadening. The size of the crystallites can be calculated from XRD patterns by a standard Scherrer analysis of the half-width of the XRD peaks. This confirms that the $La_{1-x}Eu_xMn_{0.9}Zn_{0.1}O_{3+d}$ samples prepared by the citric acid sol–gel method in the present work were indeed perovskite-type oxide materials of nanometer sizes. The average crystallite size was found to be 17·56 nm from X-ray line broadening measurements for LEMZ powder calcined at 800°C. Further, average particle diameter decreases with increasing europium content (figure 6). The average value lies in the range 16–20 nm with a very narrow size distribution.

The analysis of the lanthanum manganite powders and doped systems by EDX show a homogeneous chemical composition. In $La_{0.68}Eu_{0.32}Mn_{0.9}Zn_{0.1}O_{3+d}$, the atomic ratio La : Eu : Mn : Zn = 0·69 : 0·32 : 0·88 : 0·11 are in good agreement with the one obtained from chemical analysis (figure 7).

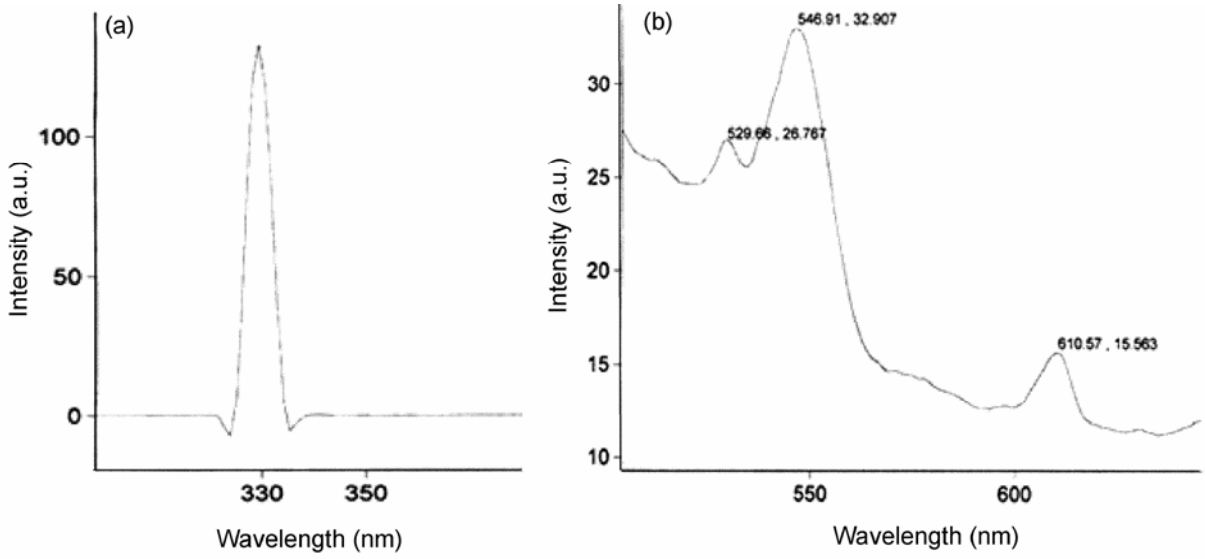

Figure 8. Excitation (**a**) (λ = 330 nm) and emission (**b**) (λ = 547 nm) spectra of $La_{0·68}Eu_{0·32}Mn_{0·9}Zn_{0·1}O_{3+d}$ nano powders annealed at 800°C.

3.4 *Luminescent properties*

$La_{0·68}Eu_{0·32}Mn_{0·9}Zn_{0·1}O_{3+d}$ nanopowders show a red emission under ultraviolet radiation. Figure 6 presents the excitation and emission spectra of $La_{0·68}Eu_{0·32}Mn_{0·9}Zn_{0·1}O_{3+d}$ nanoparticles. The excitation spectrum (figure 8a) consists of an intensive broad band with maximum at about 330 nm, which is caused by the oxygen (2*p*)-to-europium (4*f*) (Eu^{3+}–O^{2-}) charge transfer transition. Namely, the electron delocalized from the filled 2*p* shell of O^{2-} to the partially filled 4*f* shell of Eu^{3+} (Jia *et al* 2007). The emission spectrum for λ = 547 nm for $La_{0·68}Eu_{0·32}Mn_{0·9}Zn_{0·1}O_{3+d}$ sample is shown in figure 8b. The spectrum is composed of the well known europium (III) red emission lines which are assigned to transitions between the first excited state ($^5D_0$) and the ground multiplet, ^7F_J (J = 0–6). It can be seen that the main emission peak of Eu^{3+} is observed at 547 nm, while weak peaks at 530 and 610 nm were also observed. Emission bands were observed at 530, 547 and 610 nm and were attributed to the *f*–*f* transitions $^5D_0 \rightarrow {}^7F_J$ (magnetic dipole transition), $^5D_0 \rightarrow {}^7F_2$ and $^5D_0 \rightarrow {}^7F_4$ (electric dipole transitions), respectively (Tanase *et al* 2007).

4. Conclusions

Pure and single-phase with perovskite structure was formed for $La_{0·68}Eu_{0·32}Mn_{0·9}Zn_{0·1}O_{3+d}$ ($x \leq 0·32$) when the samples were sintered at 800°C for 6 h through sol–gel method. The derived Pechini method is a very simple and convenient route to obtain fine and homogeneous powders of Eu-substituted $LaMn_{0·9}Zn_{0·1}O_{3+d}$ at relatively low temperatures with a good material yield. Besides obtaining high homogeneity and purity of final products, the sol–gel method allows the structure to be controlled in a molecular scale, being totally open to incorporate other phases and the composition, density and pore morphology can be changed at various stages.

The phase of the as-prepared product is identified by XRD. The line width analysis are consistent with an average crystalline size of ~17·5 nm. The SEM study shows the ultrafine spherical particles with homogenous distribution.

Acknowledgements

This study has been supported by the Council of University of Tabriz.

References

Alemi A A, Karimpour E and Shokri H 2008 *Radiation Effects & Defects Solids* **163** 685, 893

El-Fadli Z, Metni M R, Sapina F, Martinez E, Folgado J V and Beltran A 2002 *Chem. Mater.* **14** 688

Eraoka Y, Nii H, Kagawa S, Janson K and Nygren M 2000 *Appl. Catal.* **A194** 35

Gaudon M, Labert Ch, Ansart F, Stevens Ph and Rousset A 2002 *Solid State Sci.* **4** 125

Giannakas A E, Ladavos A K and Pomonis P J 2004 *Appl. Catal. B: Environ.* **49** 147

Inaguma Y, Mashiko W, Watanabe M, Atsumi Y, Okuyama N, Katsumata T and Ohba T 2006 *Solid State Ionics* **177** 2705

Jia P Y, Lin J and Yu M 2007 *Mater. Res. Bull.* **42** 1556

Marchetti L and Forni L 1998 *Appl. Catal.* **B15** 179

Philip J and Kutty T R N 2000 *Mater. Chem. Phys.* **63** 218

Porta P, DeRossi S, Faticanti M, Minelli G, Pettiti I, Lisi L and Turco M 1999 *J. Solid State Chem.* **146** 291

Ramesha K, Smolyaninova V N, Gopalakrishnan J and Greene R L 1998 *Chem. Mater.* **10** 1436

Raveau B, Hervieu M, Maignan A and Martin C 2001 *J. Mater. Chem.* **11** 29

Reddy B K K, Rao K P and Vidyasagar K 2006 *J. Chem. Sci.* **118** 117

Rondinone A J, Samia A C S and Zhang Z J 2000 *Appl. Phys. Lett.* **76** 3624

Subias G, Garcia J, Blasco J, Proietti M G and Sanchez M C 1999 *J. Magn. Magn. Mater.* **196–197** 534

Tanase S, Galleg P M, De Gelder R and Fu W T 2007 *Inorg. Chim. Acta* **360** 102

Vazquez-Vazquez C and Lopez-Quintela M A 2006 *J. Solid State Chem.* **179** 3229

Whangbo M H, Koo H J, Villesuzanne A and Pouchard M 2002 *Inorg. Chem.* **41** 1920

Zenati R, Brrnard C, Calmet C, Guillemet S, Fantozzi G and Durand B 2005 *J. Eur. Ceram. Soc.* **25** 935

Zheng G H, Sun Y P, Zhu X B and Song W H 2006 *Phys. Lett.* **A356** 79